ORIGINAL ARTICLE

# Switching-induced stable limit cycles

**Ian A. Hiskens · Patel Bhageerath Reddy**

**Abstract** Physical limits place bounds on the divergent behaviour of dynamical systems. The paper explores this situation, providing an example where generator field-voltage limits capture behaviour, giving rise to a stable, though non-smooth, limit cycle. It is shown that shooting methods can be adapted to solve for such non-smooth switching-induced limit cycles. By continuing branches of switching-induced and smooth limit cycles, the paper established the co-existence of equilibria, smooth and non-smooth limit cycles. Furthermore, it is shown that when branches of switching-induced and smooth limit cycles merge, the limit cycles are annihilated at a grazing bifurcation.

**Keywords** Border-collision bifurcations ·
Continuation methods · Grazing · Hybrid dynamical
systems · Limit cycles · Piecewise smooth dynamics ·
Shooting methods

## 1 Introduction

The dynamic behaviour of many real-world devices and systems is subject to constraints that restrict large excursions of state variables. In some cases, the restric-
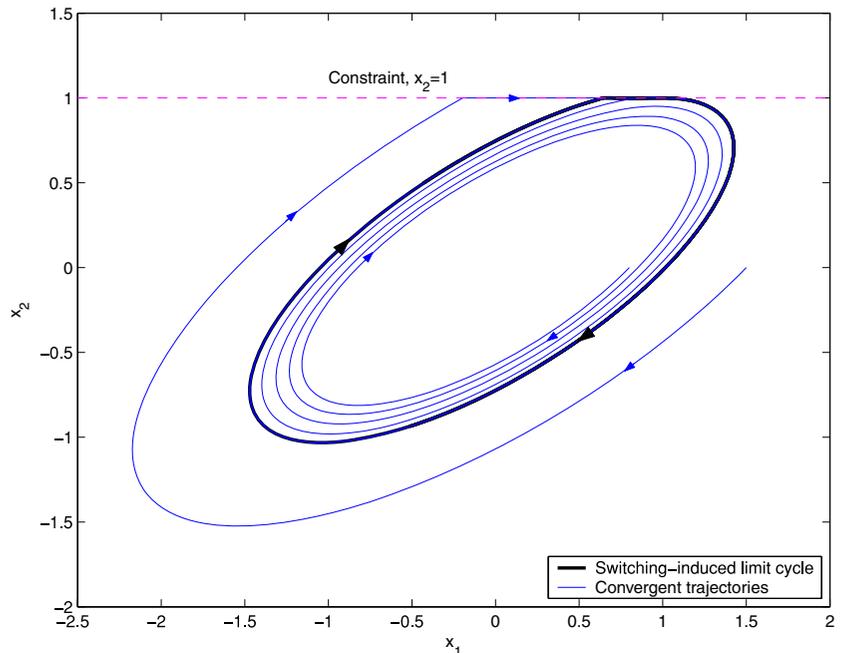
tions are inherent in the device or system's physical characteristics. In other cases, limiters are employed to avoid undesirable conditions. Generally, these restrictions can exert a significant influence on large-disturbance response. Transitions between unrestricted and restricted behaviour are often conveniently modelled via switching realizations. The resulting models involve both continuous and discrete dynamics, qualifying them as *hybrid dynamical systems* [1, 2], or *piecewise smooth dynamical systems* [3].

Constraints on large state excursions can stabilize otherwise divergent (unstable) behaviour. A very simple illustration is provided in Fig. 1. In this example, continuous dynamics are driven by an unstable second-order system. With no restriction on state behaviour, the oscillations would grow to infinity. By adding a constraint on $x_2$, however, the system stabilizes to a non-smooth limit cycle. This motivating illustration is simple, but indicative of behaviour exhibited by numerous practical systems. The paper will present a power system example, where the action of controller limits is fundamental in the creation of stable limit cycles.

It has been shown previously [4, 5] that stable limit cycles may be induced by state constraints. Furthermore, these *switching-induced* limit cycles can co-exist with other stable and unstable limit sets. Prior investigations have been impeded, however, by a lack of numerical methods for directly locating non-smooth limit cycles. Finding the limit cycle in Fig. 1 is trivial; just allow the system to run for awhile. Solving for non-smooth (possibly unstable) limit cycles in higher dimensions,

I. A. Hiskens (✉) · P. B. Reddy
Department of Electrical and Computer Engineering,
University of Wisconsin – Madison, Madison, WI 53706,
USA
e-mail: hiskens@engr.wisc.edu

**Fig. 1** Second-order system with constraint at $x_2 = 1.0$



in the presence of other limit sets, is not nearly so straightforward. Techniques that address this problem have recently been established in [6–8] though. This paper exploits these numerical *shooting methods* to further explore switching-induced non-smooth limit cycles.

The paper is organized as follows. A generic dynamic model is introduced in Section 2, along with trajectory sensitivity concepts. Section 3 provides background to limit cycle analysis and grazing phenomena, and an example is explored in Section 4. Conclusions are presented in Section 5.

## 2 System dynamic behaviour

### 2.1 Model

Analysis of hybrid system dynamics requires a non-restrictive model formulation that is capable of capturing the full range of continuous/discrete behaviour, yet is computationally efficient. It is shown in [9, 10] that these specifications are met by a model that consists of a set of differential-algebraic equations, adapted to incorporate switching of the algebraic equations, and impulsive (state reset) action. This *DA Impulsive Switched* (DAIS) model has its genesis in the familiar DAE

model

$$\dot{x} = f(x, y) \tag{1}$$

$$0 = g(x, y) \tag{2}$$

where $x \in \mathbb{R}^n$ are dynamic states, $y \in \mathbb{R}^m$ are algebraic states, $f : \mathbb{R}^{n+m} \to \mathbb{R}^n$, and $g : \mathbb{R}^{n+m} \to \mathbb{R}^m$.

Switching events can be incorporated into the DAE model by requiring the algebraic equations (2) to switch between sets of equations that describe pre- and post-event conditions. Considering a single switching event, (2) can be replaced by

$$0 = g(x, y) \triangleq \begin{cases} g^-(x, y) & s(x, y) < 0 \\ g^+(x, y) & s(x, y) > 0, \end{cases} \tag{3}$$

where the superscripts '$-$' and '$+$' index the two sets of algebraic equations.[1] A switching event coincides with a zero crossing of the trigger function $s(x, y)$. Note that the concept of crossing is important. If the trajectory just touches (grazes) the triggering surface

$$\mathcal{S} = \{(x, y) : s(x, y) = 0\} \tag{4}$$

---

[1] The functions $g^-$ and $g^+$ may themselves have a switched form, resulting in a hierarchical switching structure.

then behaviour beyond that point is indeterminant, as switching may or may not occur [7]. This is discussed further in Section 3.5. The following assumption is required for well-defined behaviour.

*Assumption 1.* The trajectory encounters the triggering surface $\mathcal{S}$ transversally.

The precise behaviour of the model at a switching event is not well defined by (3), and requires further explanation. Let the event occur at trigger time $\tau$, and define $\tau^-$ as the time instant just prior to $\tau$, and $\tau^+$ as the instant just after $\tau$. The limit values of the states can then be expressed as,

$$x^- \equiv x(\tau^-) := \lim_{t \uparrow \tau} x(t), \quad x^+ \equiv x(\tau^+) := \lim_{t \downarrow \tau} x(t)$$

(5)

$$y^- \equiv y(\tau^-) := \lim_{t \uparrow \tau} y(t), \quad y^+ \equiv y(\tau^+) := \lim_{t \downarrow \tau} y(t),$$

(6)

where $t \uparrow \tau$ implies $t < \tau$ approaches $\tau$ from below, and $t \downarrow \tau$ implies $t > \tau$ approaches $\tau$ from above. Clearly, two sets of variables $(x^-, y^-)$ and $(x^+, y^+)$ are required to fully describe behaviour at an event [11].

By definition $s(x^-, y^-) = 0$, but $s(x^+, y^+)$ may not necessarily equal zero. Furthermore, assume without loss of generality that $s(x(t), y(t)) < 0$ for $t < \tau$. Then, well-defined switching behaviour requires $s(x(t), y(t)) > 0$ for $t > \tau$. Also, this sign assumption implies $g^-(x^-, y^-) = 0$ and $g^+(x^+, y^+) = 0$. Dynamic states are unaltered at a switching event, so $x^- = x^+$. However, in order to satisfy the altered algebraic equations, often $y^- \neq y^+$.

Switching events cannot efficiently capture all forms of discrete behaviour. It is often useful to model impulsive action that introduces discrete jumps into the dynamic $x$-states. Such behaviour can be described by a reset equation

$$x^+ = h(x^-, y^-) \quad \text{when } s(x, y) = 0, \quad (7)$$

where $h \colon \mathbb{R}^{n+m} \to \mathbb{R}^n$. The superscript notation is consistent with earlier use, with $x^+$ denoting the value of $x$ just after the reset event, while $x^-$ and $y^-$ refer to the values of $x$ and $y$ just prior to the event. As in the case of a switching event, a reset event is triggered when

$s(x, y)$ passes through zero. Away from that zero crossing condition, the evolution of the dynamic $x$-states is described by the differential equations (1).

This overview of the DAIS model has neglected some of the technical details required to ensure well-defined behaviour. However, full details are provided in [9]. It should be emphasized that the DAIS model is nothing more than a formalization of simulation models that are used for practical simulation. The formalization, however, allows trajectory sensitivities to be cleanly defined [10].

Dynamic behaviour, generated numerically by simulation, can be described analytically by the *flow*,

$$x(t) = \phi(x_0, t) \tag{8}$$

$$y(t) = \psi(x_0, t). \tag{9}$$

Initial conditions imply

$$\phi(x_0, t_0) = x_0 \tag{10}$$

$$g(\phi(x_0, t_0), \psi(x_0, t_0)) = 0. \tag{11}$$

## 2.2 Trajectory sensitivities

Algorithms for locating limit cycles require the sensitivity of a trajectory (flow) to perturbations in initial conditions [12]. To obtain the sensitivity of the flows $\phi$ and $\psi$ to initial conditions $x_0$, the Taylor series expansions of (8)–(9) are formed. Neglecting higher order terms gives

$$\Delta x(t) = \frac{\partial \phi(x_0, t)}{\partial x_0} \Delta x_0 \equiv \Phi(x_0, t) \Delta x_0 \tag{12}$$

$$\Delta y(t) = \frac{\partial \psi(x_0, t)}{\partial x_0} \Delta x_0 \equiv \Psi(x_0, t) \Delta x_0 \tag{13}$$

where $\Phi$ and $\Psi$ are the *sensitivity transition matrices*, or *trajectory sensitivities*, associated with the $x$ and $y$ flows, respectively [13]. Equation (12) describes the change $\Delta x(t)$ in a trajectory, at time $t$ along the trajectory, for a given (small) change in initial conditions $\Delta x_0$. Likewise, the change in $\Delta y(t)$ is given by (13).

The evolution of the trajectory sensitivities $\Phi$ and $\Psi$ is described by variational equations that are developed in [10]. Away from events, where system dynamics evolve smoothly, the sensitivities $\Phi$ and $\Psi$ are obtained

by differentiating (1)–(2) with respect to $x_0$. This gives

$$\dot{\Phi} = f_x(t)\Phi + f_y(t)\Psi \tag{14}$$

$$0 = g_x(t)\Phi + g_y(t)\Psi \tag{15}$$

where $f_x \equiv \partial f/\partial x$, and likewise for the other Jacobian matrices. Note that $f_x$, $f_y$, $g_x$, $g_y$ are evaluated along the trajectory, and hence are time-varying matrices. The computational burden of numerically integrating this (potentially high order) linear time-varying DAE system is minimal though. It is shown in [14, 10, 15] that when an implicit numerical integration technique such as trapezoidal integration is used, the solution of (14)–(15) can be obtained as a by-product of computing the underlying trajectory.

Initial conditions for $\Phi$ are obtained from (10) as

$$\Phi(x_0, t_0) = I \tag{16}$$

where $I$ is the identity matrix. Initial conditions for $\Psi$ follow directly from (15),

$$0 = g_x(t_0) + g_y(t_0)\Psi(x_0, t_0). \tag{17}$$

Equations (14)–(15) describe the evolution of the sensitivities $\Phi$ and $\Psi$ between events. It is also necessary to determine the *jump conditions* describing event-induced changes in $\Phi$ and $\Psi$. Consider the most general case of a coincident switching/reset event, described by (3) and (7). (The jump conditions appropriate for separate switching or reset events follow directly from this more general situation.) It is shown in [10] that the jump conditions for the sensitivities $\Phi$ are given by

$$\Phi(x_0, \tau^+) = h_x^* \Phi(x_0, \tau^-) - (f^+ - h_x^* f^-)\tau_{x_0} \tag{18}$$

where

$$\tau_{x_0} \equiv \frac{\partial \tau}{\partial x_0} = -\frac{s_x^* \Phi(x_0, \tau^-)}{s_x^* f^-} \tag{19}$$

and

$$f^- \equiv f(x^-, y^-) \tag{20}$$

$$f^+ \equiv f(x^+, y^+) \tag{21}$$

$$h_x^* = \left( h_x - h_y g_y^{-1} g_x \right)\big|_{\tau^-} \tag{22}$$

$$s_x^* = \left( s_x - s_y g_y^{-1} g_x \right)\big|_{\tau^-} . \tag{23}$$

Note that jump conditions are only well defined when Assumption 1 is satisfied. Otherwise, if the trajectory encounters $\mathcal{S}$ tangentially rather than transversally, the denominator of (19) will equal zero. The sensitivities $\Psi$ immediately after the event are given by

$$\Psi(x_0, \tau^+) = -\left( g_y^{-1} g_x \right)\big|_{\tau^+} \Phi(x_0, \tau^+). \tag{24}$$

Keep in mind that $g$ in (22)–(23) refers to its pre-event form, whereas post-event conditions apply in (24).

Subsequent to the event, for $t > \tau^+$, calculation of the sensitivities proceeds according to (14)–(15). The jump conditions (18) and (24) provide the initial conditions for this post-event integration.

## 3 Limit cycle analysis

### 3.1 Poincaré maps

Limit cycles and their stability can be determined using Poincaré maps [16, 17]. This section provides a brief review of these concepts, and establishes a connection with trajectory sensitivities.

A Poincaré map effectively samples the flow of a periodic system once every period. The concept is illustrated in Fig. 2. If the limit cycle is stable, oscillations approach the limit cycle over time. The samples provided by the corresponding Poincaré map approach a fixed point. An unstable limit cycle results in divergent oscillations. For such a case, the samples of the Poincaré map diverge.
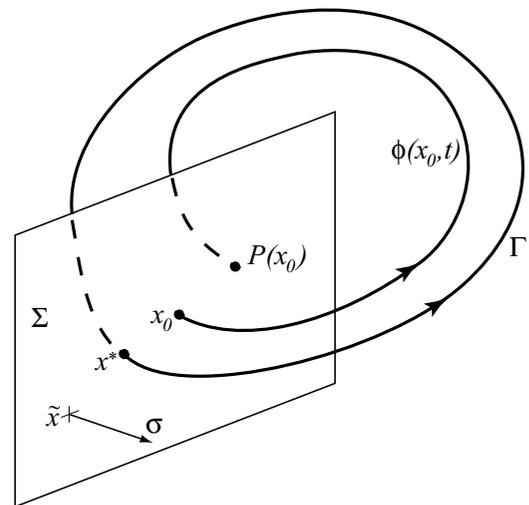
**Fig. 2** Poincaré map

To define a Poincaré map, consider the limit cycle $\Gamma$ shown in Fig. 2. Let $\Sigma$ be a hyperplane transversal to $\Gamma$ and defined by

$$\Sigma = \{x : \sigma^\top (x - \tilde{x}) = 0\} \qquad (25)$$

where $\tilde{x}$ is a point anchoring $\Sigma$, and $\sigma$ is a vector normal to $\Sigma$. The trajectory emanating from $x^*$ will again encounter $\Sigma$ at $x^*$ after $T$ seconds, where $T$ is the minimum period of the limit cycle. The existence of trajectory sensitivities ensures continuity of the flow $\phi$ with respect to initial conditions. Therefore, trajectories starting on $\Sigma$ in a neighbourhood of $x^*$ will, in approximately $T$ seconds, intersect $\Sigma$ in the vicinity of $x^*$. Hence, $\phi$ and $\Sigma$ define the Poincaré map

$$x_{k+1} = P(x_k) := \phi(x_k, \tau_r(x_k)) \qquad (26)$$

where $\tau_r(x_k) \approx T$ is the time taken for the trajectory to return to $\Sigma$. Complete details can be found in [16, 17]. Note that the Poincaré map is well defined even though the underlying flow may be non-smooth.

### 3.2 Shooting method

From (26), it can be seen that a point $x^*$ on the limit cycle can be located by using Newton's method to solve the non-linear algebraic equations

$$F_l(x^*) = \phi(x^*, \tau_r(x^*)) - x^* = 0. \qquad (27)$$

The solution process therefore has the iterative form

$$x^{i+1} = x^i - (DF_l(x^i))^{-1} F_l(x^i). \qquad (28)$$

It is shown in [7] that the Jacobian $DF_l$ is given by

$$DF_l(x^i) = \left( I - \frac{f|_{\tau_r(x^i)} \sigma^\top}{\sigma^\top f|_{\tau_r(x^i)}} \right) \Phi(x^i, \tau_r(x^i)) - I \qquad (29)$$

where $f$ is the vector field (1) and $\Phi$ is the sensitivity transition matrix (12). Referring to (27), evaluation of $F_l(x^i)$ at each iteration requires numerical integration. This process is therefore referred to as a *shooting method* [12].

Notice that because the flow $\phi$ and associated sensitivities $\Phi$ are well defined for non-smooth systems, solution of (27) is also well defined for such systems.

### 3.3 Limit cycle stability

Stability of the Poincaré map (26) is determined by linearizing $P$ at the fixed point $x^*$, i.e.,

$$\Delta x_{k+1} = DP(x^*)\Delta x_k. \qquad (30)$$

From the definition of $P(x)$ given by (26), it follows that

$$DP(x^*) = \left( I - \frac{f|_{x^*} \sigma^\top}{\sigma^\top f|_{x^*}} \right) \Phi(x^*, T) \qquad (31)$$

where $\tau_r(x^*) = T$. Even though $P$ may be built from a non-smooth trajectory, the linearization $DP$ is still well defined, and describes the local stability of the underlying non-smooth limit cycle.

The matrix $\Phi(x^*, T)$ is exactly the trajectory sensitivity matrix after one period of the limit cycle, i.e., starting from $x^*$ and returning to $x^*$. This matrix is called the *Monodromy matrix*. It is shown in [17] that for an autonomous system, one eigenvalue of $\Phi(x^*, T)$ is always 1, and the corresponding eigenvector lies along $f|_{x^*}$. The remaining eigenvalues of $\Phi(x^*, T)$ coincide with the eigenvalues of $DP(x^*)$, and are known as the *characteristic multipliers* $m_i$ of the periodic solution. The characteristic multipliers are independent of the choice of cross-section $\Sigma$.

Because the characteristic multipliers $m_i$ are the eigenvalues of the linear map $DP(x^*)$, they describe the (local) stability of the Poincaré map $P(x_k)$. Hence, the (local) stability of the periodic solution is determined by:

1. All $m_i$ lie within the unit circle, i.e., $|m_i| < 1, \forall i$. The map is stable, so the periodic solution is stable.
2. Some $m_i$ lie outside the unit circle. The periodic solution is unstable.

### 3.4 Continuation methods

It is often useful to explore the changes in limit cycle structure and stability properties that result from parameter variations. This can be achieved by introducing a free parameter $\theta$ into (27), giving

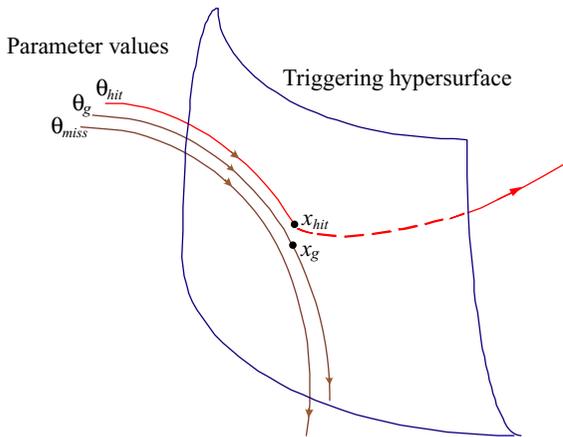$$F_l(x^*, \theta) = 0. \qquad (32)$$

**Fig. 3** Trajectory grazing triggering hypersurface

As shown earlier, the point $x^*$ given by (27) fully specifies the associated limit cycle. Therefore, the 1-manifold, or curve, defined by (32) describes the variation of $x^*$, and hence the associated limit cycle variation, with changes in parameter $\theta$.

The curve given by (32) can be traced using a homotopy method [18]. A predictor-corrector process is presented in [7]. Note that even when the underlying dynamic behaviour is non-smooth, curves given by (32) are generally smooth. Curve smoothness may be lost at grazing bifurcations though [7, 19]. The details are beyond the scope of this paper, though an illustration is provided in Section 4.

### 3.5 Grazing limit cycles

Grazing refers to situations where the trajectory just touches a triggering hypersurface. Figure 3 provides an illustration. At a parameter value $\theta_g$, lying between $\theta_{hit}$ and $\theta_{miss}$, the trajectory tangentially encounters (*grazes*) the triggering hypersurface. This bounding case separates trajectories that encounter the hypersurface from those that do not.

A grazing limit cycle must touch the target hypersurface, which can be described by[2]

$$b(x) = 0. \tag{33}$$

---

[2] The more general case of $b(x, y) = 0$ is presented in [7]. The dependence on algebraic variables $y$ is neglected here to simplify the presentation.

Furthermore, the trajectory must be tangential to the hypersurface at the point of contact. It follows from (1) and (33) that tangential contact is described by

$$\nabla b(x_g)^\top f(x_g, y_g) = 0, \tag{34}$$

as $f(x_g, y_g)$ specifies the trajectory direction at the grazing point. Collecting together appropriate equations, a grazing limit cycle is described by,

$$F_l(x^*, \theta) = 0 \tag{35}$$

$$\phi(x^*, t_g; \theta) - x_g = 0 \tag{36}$$

$$b(x_g) = 0 \tag{37}$$

$$\nabla b(x_g)^\top f(x_g, y_g) = 0 \tag{38}$$

$$g(x_g, y_g) = 0. \tag{39}$$

This set of equations can be solved using a shooting method. Full details are provided in [7], with a similar development given in [8].

## 4 Example

### 4.1 Model

A single machine infinite bus system was used to explore the existence and nature of switching-induced limit cycles. This system is shown schematically in Fig. 4, and parameter values are provided in Appendix A. The generator was represented by a sixth-order machine model [20], and the AVR/exciter by the IEEE standard model [21] given in Fig. 5. (The PSS was disabled for these studies.) This resulted in a nine-dimensional state space, $x \in \mathbb{R}^9$.

The AVR regulates the generator terminal voltage $V_t$ by adjusting the generator exciter field voltage $E_{fd}$. The
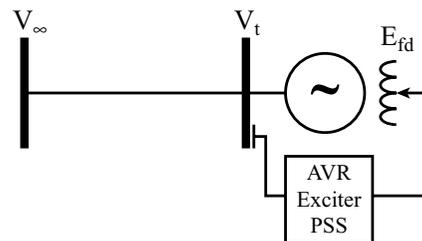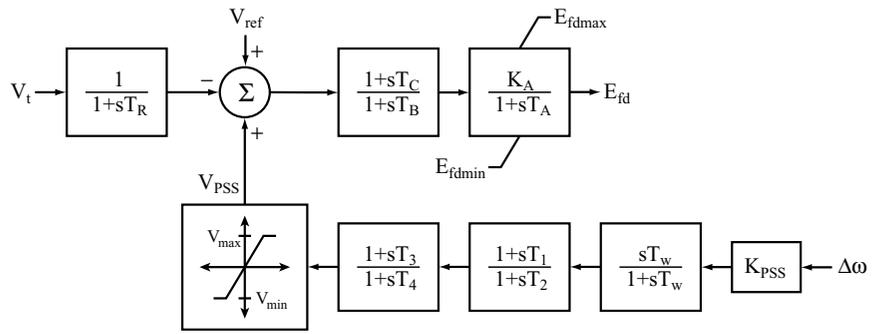


**Fig. 4** Single machine infinite bus system

**Fig. 5** Simple
PSS/AVR/exciter model



non-windup limits [22] on $E_{fd}$, shown on the output block of Fig. 5, model the physical saturation of the exciter. These limits are inherently non-smooth, with the upper limit $E_{fdmax}$ having a DAIS model of the form,

$$\dot{E}_{fd} = y_f \qquad (40)$$

$$\left.\begin{array}{l} y_f = \dfrac{1}{T_A}(K_A x_{in} - E_{fd}) \\[2mm] y_{trig} = E_{fd} - E_{fdmax} \end{array}\right\} \quad y_{trig} < 0 \qquad (41)$$

$$\left.\begin{array}{l} y_f = 0 \\[2mm] y_{trig} = K_A x_{in} - E_{fd} \end{array}\right\} \quad y_{trig} > 0, \qquad (42)$$

where $x_{in}$ is the input to the block. The model is built around two modes:

1. $E_{fd}$ is less than its upper limit. In this case $y_f$ drives $E_{fd}$ according to the block dynamics. If $E_{fd}$ encounters its upper limit, or equivalently $y_{trig}$ goes to zero, the model switches to the second mode.
2. $E_{fd}$ lies on its upper limit. In this mode, $E_{fd}$ remains fixed at its limit value as long as the block dynamics are trying to force it higher. The trigger variable $y_{trig}$ monitors the block dynamics, so this is equivalent to $y_{trig} > 0$. Constant $E_{fd}$ is achieved by setting $y_f = 0$. $E_{fd}$ can only deviate from the upper limit when the block dynamics go negative. This is reflected in $y_{trig}$ changing sign, forcing the model to switch to the first mode.

The lower limit $E_{fdmin}$ has a representation similar to (40)–(42). It will be shown that these limits restrict growing (unstable) oscillations in a way that gives rise to stable limit cycles.

This example will illustrate that the efficient computation of trajectory sensitivities for large-scale non-smooth systems allows, (1) the use of shooting methods

for locating switching-induced limit cycles, and (2) assessment of their stability properties.

### 4.2 Hopf bifurcation

For the parameter values given in Appendix A, a Hopf bifurcation occurs at an AVR gain of $K_A^* = 208.22$. The equilibrium point is unstable for $K_A > 208.22$. To illustrate, for a gain of $K_A = 212$, linearization around the equilibrium point gave an unstable eigenvalue pair of $0.0053 \pm j5.86$. The behaviour of the field voltage $E_{fd}$ is shown in Fig. 6. The initial growth in oscillation magnitude reflects the instability of the operating point. But notice that from around 70 s, behaviour stabilizes to a limit cycle. This is a consequence of the field voltage encountering its maximum limit $E_{fdmax} = 5.4$.

The shooting method was used to locate this stable limit cycle. Convergence was obtained in three iterations, with the $V_t - E_{fd}$ projection of the limit cycle shown in Fig. 7. It was found that all characteristic multipliers lay within the unit circle, with the largest having a magnitude of 0.83. This confirmed the limit cycle was indeed an attractor.

Further investigation of the Hopf bifurcation revealed that it was in fact supercritical. The bifurcation diagram of Fig. 8, produced using the continuation process of Section 3.4, shows a branch of stable limit cycles emanating from the Hopf bifurcation.[3] This branch of limit cycles undergoes a cyclic fold at $K_A = 209.9$, beyond which the branch comprises unstable limit cycles.

As shown in Fig. 8, the stable non-smooth limit cycles, induced by the $E_{fdmax}$ limit, co-exist

---

[3] The limit cycles are represented in Fig. 8 by the extreme values of $E_{fd}$.

**Fig. 6** Response of field
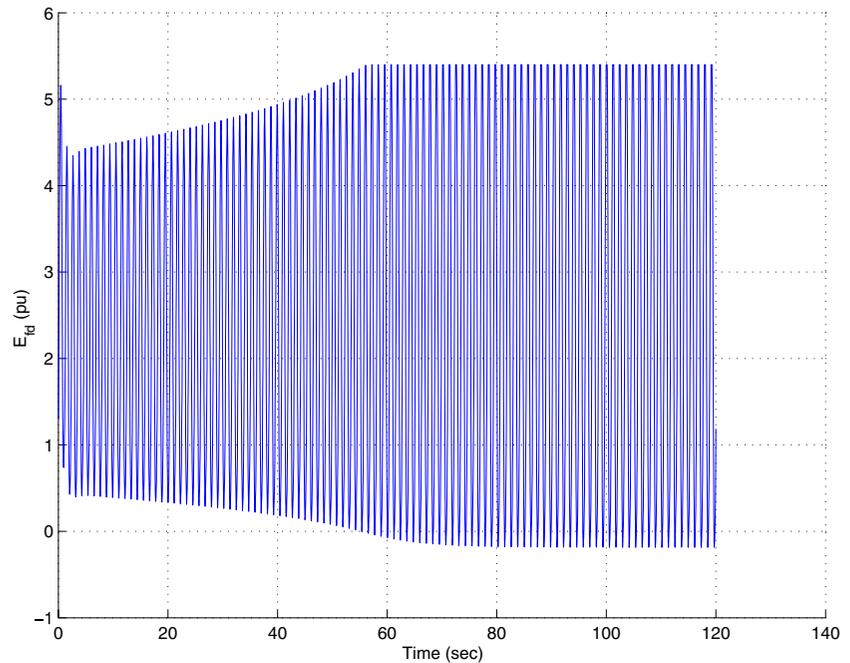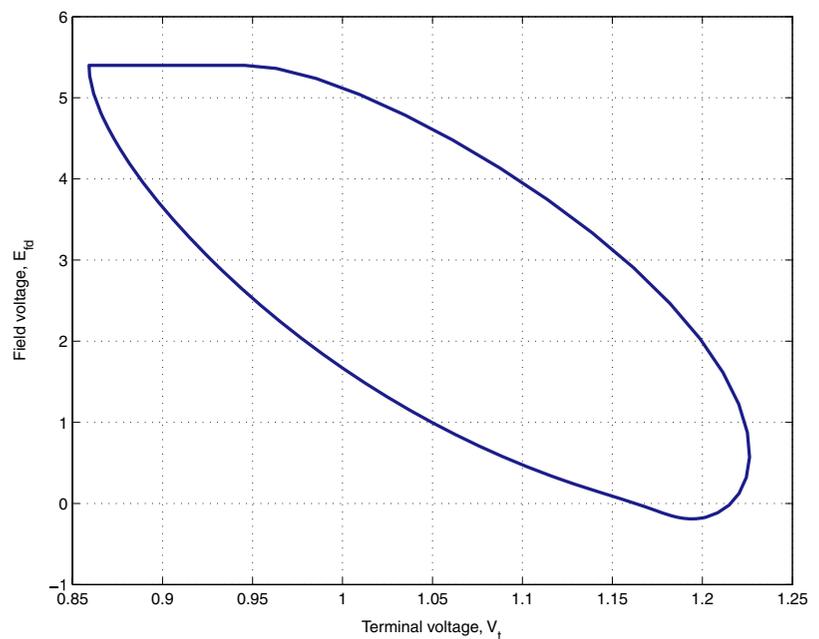voltage $E_{\text{fd}}$ for $K_A = 212$



**Fig. 7** Stable limit-induced
limit cycle for $K_A = 212$



with the smooth limit cycles that result from the
Hopf bifurcation. Over the range $208.22 < K_A <
209.9$, the system exhibits an unstable equilib-
rium point, an unstable limit cycle, and two sta-
ble limit cycles (one smooth and one non-smooth).
These limit sets are shown in Fig. 9, for a gain
$K_A = 209$.

The shooting method of Section 3.2 was used to ob-
tain the limit cycles of Fig. 9. In all cases, convergence
was obtained in three iterations, with each iteration re-
quiring a single simulation of one period of the os-
cillation. On the other hand, reliance on time-domain
simulation would be futile. The unstable limit cycle
has characteristic multipliers both inside and outside

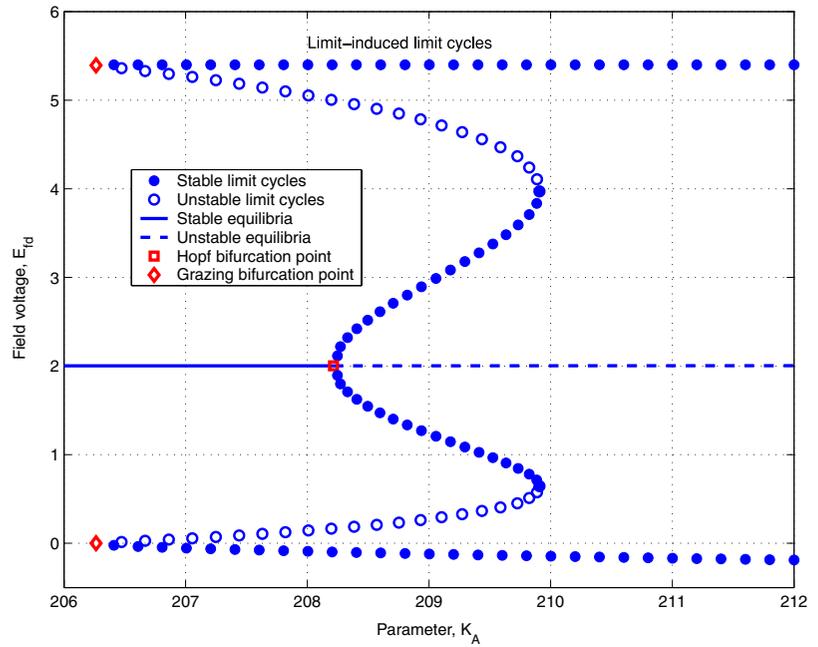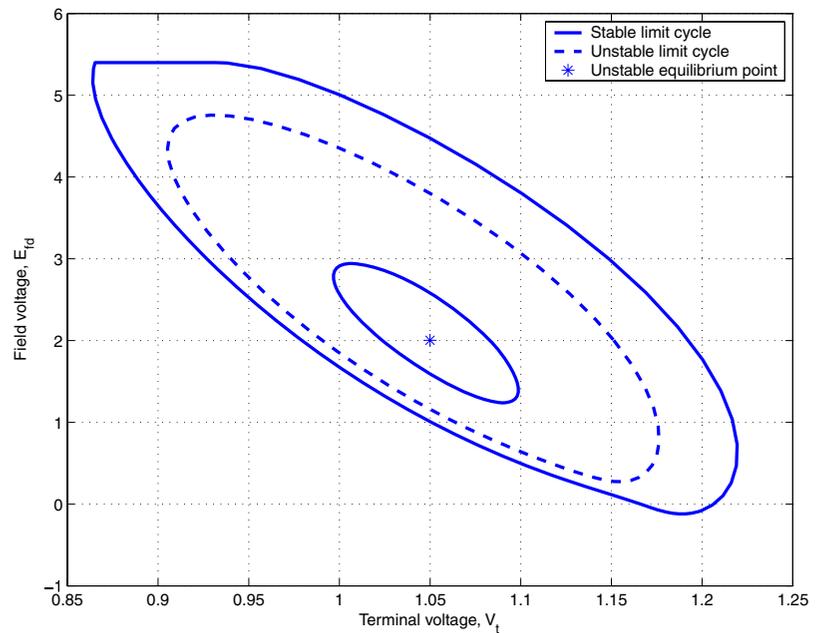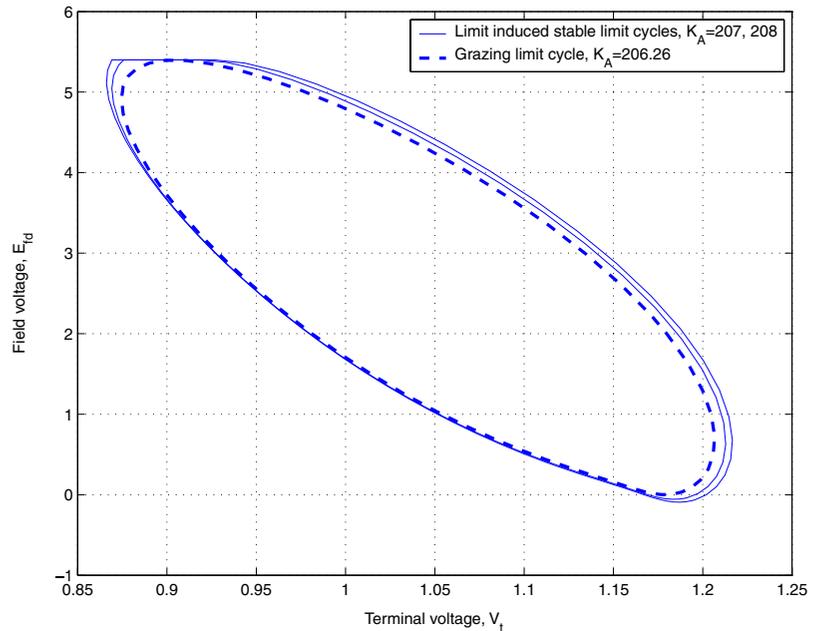**Fig. 8** Bifurcation diagram



**Fig. 9** Co-existing limit cycles and equilibrium point, $K_A = 209$



the unit circle, so time reversal would not achieve convergent behaviour. Furthermore, transient behaviour is poorly damped in the vicinity of the Hopf bifurcation. Therefore, lengthy simulation would be required for adequate convergence to the stable limit cycles. Shooting methods are however unaffected by the stability properties and damping associated with a limit cycle.

### 4.3 Grazing bifurcation

As the gain $K_A$ is reduced, the branches of switching-induced and smooth limit cycles converge to a point where the smooth limit cycle becomes tangential to (grazes) the $E_{\text{fdmax}}$ surface. By solving (35)–(39) using the shooting method of [7], it was found that the grazing

**Fig. 10** Grazing limit cycle



limit cycle occurred at $K_A = 206.26$. This limit cycle is shown in Fig. 10. The figure also shows that as $K_A$ reduces, the switching-induced limit cycle spends less and less time on the $E_{fdmax}$ surface. Correspondingly, one of its characteristic multipliers approaches unity. The smooth and non-smooth limit cycles coalesce at grazing. As $K_A$ is further reduced beyond the grazing value, the limit cycles vanish, with structural stability lost due to a grazing bifurcation [19, 23].

The grazing bifurcation observed in this example has a form similar to grazing-sliding bifurcations discussed in [24]. In this case, however, there is no sliding. Rather, the switching dynamics (40)–(42) produce behaviour that achieves an outcome similar to the Filippov (sliding) solution. (Note that the DAIS representation allows more general hybrid system structures than those usually associated with piecewise-smooth systems.)

The Poincaré maps of the bifurcating limit cycles together establish a piecewise-smooth map, with the grazing case forming the border between the smooth regions of the composite map. In terms of this piecewise-smooth map, the grazing bifurcation may be interpreted as a border-collision bifurcation [19, 25, 26]. At the bifurcation, a branch of stable fixed points encounters a branch of unstable fixed points. No fixed points exist for values of the parameter $K_A$ beyond the bifurcation value. The example therefore exhibits a saddle-node

border-collision bifurcation. This is consistent with the observation that a characteristic multiplier approaches unity as the stable branch is traversed towards the bifurcation.

## 5 Conclusions

The flow of a dynamical system, and the associated trajectory sensitivities, are well defined for smooth systems. These concepts can, however, be extended in a natural way to non-smooth systems. Accordingly, Poincaré maps also extend naturally to non-smooth systems. This allows a straightforward development of shooting methods and local stability analysis for non-smooth limit cycles.

The extensions break down when a trajectory tangentially encounters (grazes) a triggering hypersurface. These grazing situations can be located though by solving, via a shooting method, an augmented problem that includes the limit cycle description together with the conditions governing the tangential encounter.

Constraints on large state excursions are inherent in many real-world devices and systems. The resulting restrictions on system dynamics can stabilize otherwise divergent (unstable) behaviour. For systems that exhibit underlying oscillatory response, constraints tend

to induce periodic, non-smooth, limit cycle behaviour. A power system example, which gives rise to this form of behaviour, has been explored in the paper. It has been shown that switching-induced limit cycles can co-exist with other, more traditional, limit sets.

As parameters vary, switching-induced limit cycles may vanish at grazing bifurcations, where the flow becomes tangential to the switching surface. An example presented in the paper shows the annihilation of a switching-induced limit cycle and a smooth limit cycle at such a bifurcation. Using Poincaré maps, this form of grazing phenomenon can be interpreted as a saddle-node border-collision bifurcation.

## Appendix A: Example parameters

The following per unit parameter values fully describe the single machine infinite bus system of Section 4. All parameters are given on a 100 MVA base, with $\omega$ in rad/s.

- Machine parameters: $r_a = 0.0006$, $x_d = 0.588$, $x'_d = 0.0913$, $x''_d = 0.075$, $T'_{d0} = 6.59$, $T''_{d0} = 0.0386$, $x_q = 0.588$, $x'_q = 0.1$, $x''_q = 0.075$, $T'_{q0} = 1.0$, $T''_{q0} = 0.0419$, $x_l = 0.049$, $M = 0.0667$, $D = 0.005$, $T_m = 2.5$.
- AVR parameters: $T_R = 0.04$, $T_A = 0.04$, $T_B = 12$, $T_C = 1$, $V_{setpoint} = 1.05$, $E_{fdmax} = 5.4$, $E_{fdmin} = -5$.
- PSS is disconnected.
- Infinite bus parameters: $V_\infty = 1$.
- Line parameters: $r = 0.01$, $x = 0.25$, $b = 0.4$.

## References

1. van der Schaft, A., Schumacher, H.: An Introduction to Hybrid Dynamical Systems. Springer-Verlag, London (2000)
2. Liberzon, D.: Switching in Systems and Control. Birkhauser, Boston (2003)
3. di Bernardo, M., Chung, H.S., Tse, C.K.: Guest editorial: Special issue on switching and systems. IEEE Trans. Circuits Syst. I: Fundamental Theory Appl. **50**(8), 973–974 (2003)
4. Jiang, X., Schattler, H., Zaborszky, J., Venkatasubramanian, V.: Hard limit induced oscillations. In: Proceedings of the IEEE International Symposium on Circuits and Systems, Seattle, Washington (May 1995)
5. Howell, F., Venkatasubramanian, V.: Transient stability assessment with unstable limit cycle approximation. IEEE Trans. Power Syst. **14**(2), 667–677 (1999)
6. Hiskens, I.A.: Stability of hybrid system limit cycles: Application to the compass gait biped robot. In: Proceedings of the 40th IEEE Conference on Decision and Control, Orlando, FL (December 2001)
7. Donde, V., Hiskens, I.A.: Shooting methods for locating grazing phenomena in hybrid systems. Int. J. Bifurcation Chaos **16**(3), 671–692 (2006)
8. Zhao, X., Dankowicz, H.J., Reddy, C.K., Nayfeh, A.H.: Modeling and simulation methodology for impact microactuators. J. Micromech. Microeng. **14**, 775–784 (2004)
9. Hiskens, I.A.: Power system modeling for inverse problems. IEEE Trans. Circuits Syst. I: Regular Papers **51**(3), 539–551 (2004)
10. Hiskens, I.A., Pai, M.A.: Trajectory sensitivity analysis of hybrid systems. IEEE Trans. Circuits Syst. I: Fundamental Theory Appl. **47**(2), 204–220 (2000)
11. Lee, E.A., Zheng, H.: Operational semantics of hybrid systems. In: Hybrid Systems: Computation and Control. Lecture Notes in Computer Science, Morari, M., Thiele, L. (eds.) Vol. 3414, pp. 25–53. Springer, Berlin (2005)
12. Stoer, J., Bulirsch, R.: Introduction to Numerical Analysis, 2nd edn. Springer, New York (1993)
13. Frank, P.M.: Introduction to System Sensitivity Theory. Academic Press, New York (1978)
14. Feehery, W.F., Tolsma, J.E., Barton, P.I.: Efficient sensitivity analysis of large-scale differential-algebraic systems. Appl. Numer. Math. **25**, 41–54 (1997)
15. Li, S., Petzold, L., Zhu, W.: Sensitivity analysis of differential-algebraic equations: a comparison of methods on a special problem. Appl. Numer. Math. **32**(8), 161–174 (2000)
16. Seydel, R.: Practical Bifurcation and Stability Analysis, 2nd edn. Springer-Verlag, New York (1994)
17. Parker, T.S., Chua, L.O.: Practical Numerical Algorithms for Chaotic Systems. Springer-Verlag, New York, NY (1989)
18. Garcia, C.B., Zangwill, W.I.: Pathways to Solutions, Fixed Points and Equilibria. Prentice Hall, Englewood Cliffs, NJ (1981)
19. di Bernardo, M., Budd, C.J., Champneys, A.R.: Grazing and border-collision in piecewise-smooth systems: A unified analytical framework. Phys. Rev. Lett. **86**(12), 2553–2556 (2001)
20. Sauer, P.W., Pai, M.A.: Power System Dynamics and Stability. Prentice Hall, Upper Saddle River, NJ (1998)
21. IEEE Std 421.5-1992: IEEE Recommended Practice for Excitation System Models for Power System Stability Studies. Institute of Electrical and Electronics Engineers, Inc., New York (1992)
22. Goodwin, G., Graebe, S., Salgado, M.: Control System Design. Prentice Hall, Upper Saddle River, NJ (2001)
23. Fredriksson, M.H., Nordmark, A.B.: Bifurcations caused by grazing incidence in many degrees of freedom impact oscillators. Proc. R. Soc. Lond. A **453**(1961), 1261–1276 (1997)
24. di Bernardo, M., Kowalczyk, P., Nordmark, A.B.: Bifurcations of dynamical systems with sliding: derivation of normal-form mappings. Phys. D **170**, 175–205 (2002)
25. Nusse, H.E., Ott, E., Yorke, J.A.: Border-collision bifurcations: an explanation for observed bifurcation phenomena. Phys. Rev. E **49**(2), 1073–1077 (1994)
26. Banerjee, S., Hassouneh, M.A.: Bifurcation phenomena in hybrid dynamical systems. In: Proceedings of the IEEE International Symposium on Circuits and Systems, Bangkok, Thailand. Tutorial Guide, Vol. 2, pp. 37–46 (2003)